Int. J. Heat Mass Transfer. Vol. 23, pp. 17–26
Pergamon Press Ltd. 1980. Printed in Great Britain

RADIATIVE ABSORPTION BY EVAPORATING DROPLETS

G. M. HARPOLE
School of Engineering and Applied Science, University of California, Los Angeles, CA 90024, U.S.A.

(*Received* 22 *June* 1978 *and in revised form* 29 *January* 1979)

Abstract—The volumetric heating due to radiation absorption has been computed as a function of radial position for spherical water droplets in black body surrounds of temperatures up to 1450 K. The droplet effective absorptance and the time to evaporate from a reference diameter to any smaller diameter have also been computed and tabulated. By taking differences between entries in the table, the time to evaporate from one size to another size can be found. The ray tracing procedure developed for these computations includes polarization, refraction, external reflection, multiple internal reflections, and absorption.

NOMENCLATURE

a, imaginary part of the propagation vector;
A, droplet surface area;
A_c, droplet cross sectional area, πR^2;
B, superheat parameter, $c_p(T_v - T_{sat})/(h_{f_g} - q_r/\dot{m}'')$;
c, speed of light in a vacuum [2.997925×10^8 m/s];
c_d, drag coefficient, $d/(\frac{1}{2}\rho_v U^2 A_c)$;
c_p, heat capacity at constant pressure;
d, drag;
D, droplet diameter;
E, electric field vector;
F, generalized Snell's law parameter;
g, gravitational acceleration [9.80665 m/s^2];
h, Planck's constant [6.6256×10^{-34} J s^{-1}];
h_{fg}, heat of fusion;
H, magnetic field vector;
I, intensity;
k, thermal conductivity;
k, real part of the propagation vector;
k_c, Boltzmann constant [1.38054×10^{-23} J K^{-1}];
K, absorption coefficient;
L, parallel layer thickness;
$\dot{m}''$, surface mass flux;
n, real part of $\tilde{n}$;
$\tilde{n}$, complex refractive index, $n - i\kappa$;
Nu_D, Nusselt number, $q_c D/k(T_v - T_{sat})$;
Pr, Prandtl number, $\mu c_p/k$;
q, heat flux;
Q, power;
r, radial position;
$\tilde{r}$, Fresnel coefficient;
R, droplet radius;
Re, real part of;
Re_D, Reynolds number, $\rho_v U D/\mu$;
s, distance along a ray;
t, time;
T, temperature;
U, relative velocity;
V, complex propagation vector, $\mathbf{k} - i\mathbf{a}$;
x, size parameter, $\pi D/\lambda$;
$\ddot{x}$, acceleration.

Greek symbols

α, absorptance;
α_1, absorption of a ray in one traversal;
θ, incident ray angle, angle;
κ, negative imaginary part of $\tilde{n}$;
λ, wave length in a vacuum;
μ, dynamic viscosity;
ν, wavenumber in a vacuum;
ρ, reflectivity, density;
σ, Stefan–Boltzmann constant [5.6697×10^{-8} W/m^2 K^4];
ϕ, initial refracted angle;
ω, frequency;
Ω, solid angle.

Subscripts

abs, absorbed;
B, black body;
c, convective;
eff, effective;
i, of the incident side;
l, of the liquid;
0, initial;
r, of the refracted side, radiative;
sat, of saturation;
v, of the ambient vapor;
$\perp$, of the perpendicular polarization component;
$\parallel$, of the parallel polarization component.

Superscripts

*, complex conjugate of;
^, unit vector;
$^+$, without blowing;
~, a complex quantity.

INTRODUCTION

SPRAYS of droplets are heated in numerous industrial processes such as in combustion sprays, spray cooling, and spray drying. The evaporation of these sprays is most commonly analyzed by assuming that each droplet behaves independently from the others [1–5]. Droplets are grouped by their size range, and evaporation within a group is determined from the single droplet heat-transfer coefficient of the average droplet size in that group. Radiative transfer to droplets is rarely included in such computations, yet in situations with very high temperature surrounds, such as in various postulated nuclear reactor accident scenarios, the radiative transfer can be even more significant than the convective transfer.

During the "rewetting" or "reflood" portions of a hypothetical Loss of Coolant Accident, water droplets are enclosed by hot dry closely spaced fuel rods which have overall emissivities between 0.7 and 0.8 [6]. In such an enclosure, droplet radiative absorption should be computed assuming each droplet has uniform black body surrounds.

The exact solution to Maxwell's equations for an electromagnetic wave incident upon a sphere with a complex index of refraction (i.e. absorbing sphere) was formulated by Mie [7]. Mie theory has been used to compute absorption by spheres with various constant values of the complex index of refraction [8–11]. However, it is too expensive to compute enough absorption values to integrate over frequency for the strongly frequency dependent and band-like complex index of refraction of water (see Fig. 1). There is an asymptotic approximation to Mie theory for the absorptance of large or moderate sized spheres [8],

$$\alpha = 1 + 2\exp(-4x\kappa)/4x\kappa + 2[\exp(-4x\kappa) - 1]/(4x\kappa)^2, \quad (1)$$

where $x = \pi D/\lambda$ is the size parameter, D is the diameter, λ is the wavelength, and κ is the negative imaginary part of the refractive index. Unfortunately, the derivation of equation (1) also assumes that κ is small and that the real part of the index of refraction, n, is close to one.

Chan and Grolmes [12] suggest that equation (1) could be used for water droplet absorption computations. However, Plass [9] graphed equation (1) along with exact Mie theory solutions for comparison, with the size parameter ranging from 0 to 28, the real part of the refractive index being 1.33, and the imaginary part 0.0001, 0.01, and 0.1. Ray optics computations deviate from exact Mie theory only about half as much as equation (1) does for the cases considered by Plass. In the limit of very large droplets, ray optics show that the external reflection is about 7%, while because of the refractive index assumptions, equation (1) shows no external reflection.

Mie's theory can be approximated with ray optics when the sphere diameter is much larger than the wavelength of the radiation. For excellent quantitative agreement between the two theories on fine details such as the angular scattering distribution including rainbows and glories, the size parameter must be greater than 400 [13]. For the absorption cross section, however, ray optics gives good results if the size parameter is greater than 30 [9–11]. For a black body intensity distribution of temperature T_B, if DT_B is greater than 100 [mm K], the size parameter would be above 30 for the bulk of radiation, and error in the ray-tracing absorption computation is less than 5%. The effects of resonances tend to cancel for such a continuous intensity distribution.

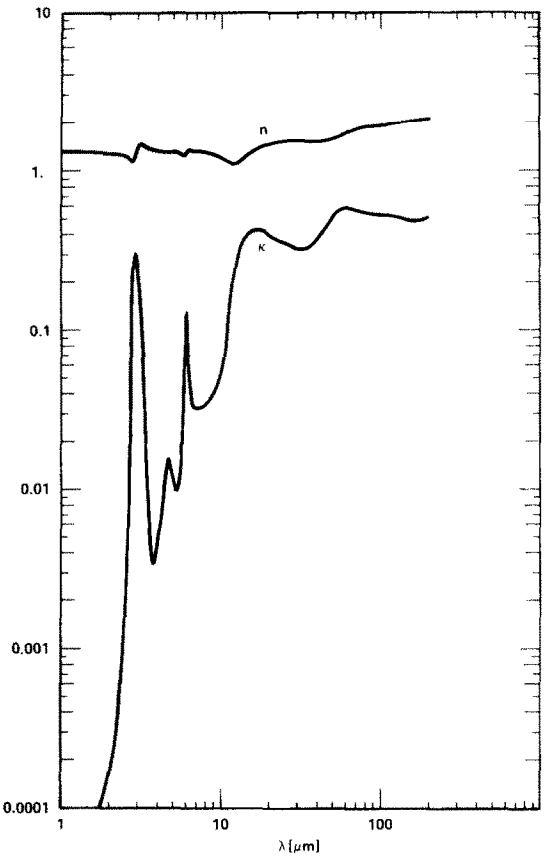

FIG. 1. Complex refractive index of water [15].

Ray tracing has been used previously to compute absorption by spheres irradiated at single wavelengths [14]. Refraction and external reflection were included, but they were computed based on only the real part of the index of refraction. Refraction focuses the rays towards the sphere center, but the rays are attenuated as they travel through the sphere. Thus, the volumetric heating is higher near the center for weakly absorbing or small spheres, but the volumetric heating is higher near the surface for strongly absorbing or large spheres.

The complex refractive index of water at room temperature (298 K) as a function of wavelength is well established in the infrared [15–17]. The complex refractive index of water at higher temperatures [17, 18] is not substantially different for the present

purposes from that at room temperature. The more reliable and complete 298 K values [15] have been used in the present work (see Fig. 1).

RAY TRACING IN AN ABSORBING MEDIUM

The refracted angle of a plane wave encountering a semi-infinite absorbing medium depends on the imaginary part of the refractive index as well as the real part. The absorption actually has some dependence on the refracted angle. If a complex propagation vector is defined as

$$\mathbf{V} = \mathbf{k} - i\mathbf{a}, \tag{2}$$

then the components of the refracted wave can be written as

$$\mathbf{E} = \mathbf{E}_0 e^{i(\omega t - \mathbf{V}\cdot\mathbf{r})} = \mathbf{E}_0 e^{-\mathbf{a}\cdot\mathbf{r}} e^{i(\omega t - \mathbf{k}\cdot\mathbf{r})} \tag{3a}$$

$$\mathbf{H} = \mathbf{H}_0 e^{i(\omega t - \mathbf{V}\cdot\mathbf{r})} = \mathbf{H}_0 e^{-\mathbf{a}\cdot\mathbf{r}} e^{i(\omega t - \mathbf{k}\cdot\mathbf{r})}, \tag{3b}$$

where $\mathbf{r}$ is an arbitrary position vector. The incident wave components are of this same form, and so the matching condition

$$\mathbf{V}_i \cdot \mathbf{r} = \mathbf{V}_r \cdot \mathbf{r} \tag{4}$$

must hold for $\mathbf{r}$ along the interface, where the subscripts i and r denote of the incident wave and of the refracted wave, respectively. Noting that $\mathbf{a}$ is zero in the incident (non-absorbing) medium, the real and imaginary parts of matching condition (4) result in the two relations

$$k_i \sin\theta_i = k_r \sin\theta_r \tag{5a}$$

$$\mathbf{a}_r \cdot \mathbf{r} = 0, \tag{5b}$$

where k_i and k_r are $|\mathbf{k}_i|$ and $|\mathbf{k}_r|$, respectively. Thus, $\mathbf{a}$ is normal to the interface, while $\mathbf{k}$ is in the direction of propagation.

The magnitudes of the propagation vector components, a and k, can be found from the wave equation,

$$\nabla^2 E = \frac{\tilde{n}^2}{c^2}\frac{\partial^2 E}{\partial t^2} \tag{6}$$

where $\tilde{n} = n - i\kappa$ is the complex refractive index and c is the speed of light in a vacuum. For plane harmonic waves we have $\nabla\psi = -i\mathbf{V}\psi$ and $\partial\psi/\partial t = i\omega\psi$, so that the wave equation becomes

$$(\mathbf{k} - i\mathbf{a})\cdot(\mathbf{k} - i\mathbf{a}) = (n - i\kappa)^2 k_0^2, \tag{7}$$

where k_0 is defined as ω/c. The real and imaginary parts of equation (7) supply two relations with the two unknowns a and k. Thus, equation (7) results in

$$a = \frac{n\kappa k_0^2}{k\cos\theta} \tag{8}$$

and

$$\frac{k}{k_0} = \left\{\tfrac{1}{2}(n^2 - \kappa^2) + \tfrac{1}{2}\left[(n^2-\kappa^2)^2 + 4\left(\frac{n\kappa}{\cos\theta}\right)^2\right]^{1/2}\right\}^{1/2}. \tag{9}$$

Moreover, since equation (9) must hold separately in both media, equations (5a) and (9) can be combined as

$$\{(n_i^2 - \kappa_i^2) + [(n_i^2 - \kappa_i^2)^2 + 4(n_i\kappa_i/\cos\theta_i)^2]^{1/2}\}^{1/2} \sin\theta_i = \{(n_r^2 - \kappa_r^2) + [(n_r^2 - \kappa_r^2)^2 + 4(n_r\kappa_r/\cos\theta_r)^2]^{1/2}\}^{1/2} \sin\theta_r. \tag{10}$$

This modified Snell's law was derived previously by Bell *et al.* [19]. Equation (10) can be arranged in the form

$$\sin\theta_r = [(n_i/n_r)\sin\theta_i] F(n_i, \kappa_i, n_r, \kappa_r, \theta_i), \tag{11}$$

where for $n_i = 1$ and $\kappa_i = 0$, dropping the r subscript,

$$F = \left[\frac{-(n^2 - \kappa^2 + \sin^2\theta_i) + \{(n^2 - \kappa^2 + \sin^2\theta_i)^2 + 4[n^2\kappa^2 - (n^2 - \kappa^2)\sin^2\theta_i]\}^{1/2}}{2\left[\kappa^2 - \left(1 - \frac{\kappa^2}{n^2}\right)\sin^2\theta_i\right]}\right]^{1/2}. \tag{12}$$

The power crossing a unit area perpendicular to the propagation direction is given by the Poynting theorem [20] as

$$I d\Omega \hat{\mathbf{s}} = \tfrac{1}{2}\mathrm{Re}(\mathbf{E}\times\mathbf{H}^*) = \tfrac{1}{2}(\mathbf{E}_0 \times \mathbf{H}_0) e^{-2\mathbf{a}\cdot\mathbf{s}} \tag{13}$$

where $\mathbf{s}$ is a position vector in the propagation direction and where $\hat{\mathbf{s}}$ is a unit vector. $\mathbf{E}_0$, $\mathbf{H}_0$, and $\hat{\mathbf{s}}$ are mutually perpendicular, so that

$$I d\Omega = \tfrac{1}{2} E_0 H_0 e^{-2\mathbf{a}\cdot\mathbf{s}}. \tag{14}$$

To find the absorbed fraction of the incident wave intensity, we need only concern ourselves with the $e^{-2\mathbf{a}\cdot\mathbf{s}}$ decay. From equation (8)

$$-2\mathbf{a}\cdot\mathbf{s} = -2sn\kappa(\omega/c)(k_0/k), \tag{15}$$

and since

$$\omega = 2\pi\nu = \frac{2\pi c}{\lambda}, \tag{16}$$

where λ is the wavelength in a vacuum, the ray intensity is diminished as

$$I = I_0 e^{-2\mathbf{a}\cdot\mathbf{s}} = I_0 e^{-Ks}, \tag{17a}$$

where

$$K = (4\pi\kappa/\lambda)(nk_0/k). \tag{17b}$$

K has a weak dependence on the refracted angle as can be seen from equations (9) and (17b). This exponential decay coefficient is different from the decay coefficient for a plane wave in a single medium [21] by the factor (nk_0/k). This factor is not seen elsewhere in the literature because other derivations of equations similar to these have not included both

absorbing materials and real non-normal angles. This factor is one for a wave of normal incidence; the factor also becomes unity in the $\kappa^2 \ll n^2$ limit.

The reflected intensity fraction of a plane wave encountering a plane surface is obtained from the Fresnel coefficients [20]

$$\tilde{r}_\perp = \frac{\tilde{n}_r \cos\tilde{\theta}_i - \tilde{n}_i \cos\tilde{\theta}_r}{\tilde{n}_r \cos\tilde{\theta}_i + \tilde{n}_i \cos\tilde{\theta}_r} \tag{18a}$$

$$\tilde{r}_{||} = \frac{\tilde{n}_i \cos\tilde{\theta}_i - \tilde{n}_r \cos\tilde{\theta}_r}{\tilde{n}_i \cos\tilde{\theta}_i + \tilde{n}_r \cos\tilde{\theta}_r}. \tag{18b}$$

The reflected fractions of the perpendicular and parallel components are then

$$\rho_\perp = \tilde{r}_\perp \tilde{r}_\perp^* \quad \text{and} \quad \rho_{||} = \tilde{r}_{||} \tilde{r}_{||}^*, \tag{19}$$

respectively. Typically, either $\tilde{\theta}_i$ or $\tilde{\theta}_r$ will be a known real angle (the angle on the non-absorbing side), and the cosine of the other angle is obtained from the relation $\cos\tilde{\theta} = (1 - \sin^2\tilde{\theta})^{1/2}$, using Snell's law in the form

$$\tilde{n}_i \sin\tilde{\theta}_i = \tilde{n}_r \sin\tilde{\theta}_r. \tag{20}$$

Note that the—not physically meaningful—complex refracted angle $\tilde{\theta}_r$, and the real refracted angle θ_r, are different, and thus equations (11) and (20) are two different forms of Snell's law.

In using ray theory, it is assumed that surfaces act locally flat and that all waves act locally as though they were plane waves. The rays are in the wave propagation direction, and they have the local wave intensity. In tracing a single ray through a droplet (see Fig. 2), from the incident angle θ, equations (11) and (12) are used to find the initial refracted angle ϕ. By symmetry, ϕ becomes the incident angle for all internal reflections, and $D\cos\phi$ is the distance travelled between consecutive surface encounters. The fraction of the remaining ray intensity absorbed in one such traversal is

$$\alpha_1 = 1 - e^{-KD\cos\phi}. \tag{21}$$

The reflected intensity fraction, ρ, of an exterior ray first encountering the droplet surface is found from equations (18)–(20). For surface encounters by an internal ray, θ will be the refracted angle, due to interchangeability of the i and r subscripts in equation (10). The reflected intensity fraction on each of these internal ray encounters with the surface is found to be identical to that for the initial external reflection. However, this reflectivity for the perpendicular polarized ray component, $\rho_\perp$, is different from that for the parallel component, $\rho_{||}$.

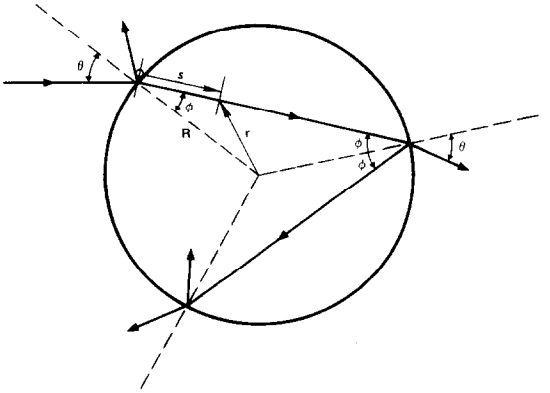

FIG. 2. Droplet ray tracing.

To compute the absorbed fraction of a single ray incident upon the droplet, the absorption in the infinite series of traversals between internal reflections must be summed. For the perpendicularly polarized components, $\alpha_1(1-\rho_\perp)[\rho_\perp(1-\alpha_1)]^{n-1}$ is the fraction of the initial intensity which is absorbed on the nth traversal. The same infinite geometric series holds for the parallel component with $\rho_\perp$ replaced by $\rho_{||}$. The total absorbed fraction is obtained by summing the series, which after averaging the perpendicular and parallel component absorptions, assuming initially equal perpendicular and parallel component intensities outside the droplet, results in

$$\alpha = \tfrac{1}{2}\left[\frac{\alpha_1(1-\rho_\perp)}{1-\rho_\perp(1-\alpha_1)} + \frac{\alpha_1(1-\rho_{||})}{1-\rho_{||}(1-\alpha_1)}\right]. \tag{22}$$

In the limit of strong absorption (i.e. large KD or α_1 approaching unity) the droplet absorbs all radiation that is initially transmitted through the droplet surface

$$\lim_{\alpha_1 \to 1} \alpha = 1 - \tfrac{1}{2}(\rho_\perp + \rho_{||}). \tag{23}$$

In the limit of weak absorption (i.e. small KD or α_1 approaching zero) α approaches α_1.

Absorption of single rays by a droplet must be weighted with the incident power distribution and integrated over solid angle and wavenumber to obtain the total absorbed power per unit droplet surface area. The differential power distribution is

$$d^5Q = I(\nu)\cos\theta\, d^2\Omega\, d\nu\, d^2A, \tag{24}$$

where I is the intensity distribution, Ω is solid angle and A is droplet surface area. For a uniformly irradiated droplet, the absorbed power is

$$Q_{abs} = 2\pi^2 D^2 \int_0^\infty I(\nu)\left[\int_0^{\pi/2} \alpha(\nu,\theta)\cos\theta\sin\theta\, d\theta\right] d\nu. \tag{25}$$

For black body radiation, the intensity distribution is

$$I = I_B = \frac{2hc^2\nu^3}{\exp(hc\nu/k_c T_B) - 1} \tag{26}$$

where h is Planck's constant and k_c is the Boltzmann constant. The effective absorptance of a droplet is the ratio of absorbed power to incident power

$$\alpha_{eff} = Q_{abs}/Q_i \tag{27}$$

where the incident power is given by

$$Q_i = \pi^2 D^2 \int_0^\infty I(\nu)\, d\nu. \tag{28}$$

For a black body intensity distribution, $Q_i = \pi D^2 \sigma T_B^4$, where σ is the Stefan–Boltzmann constant. The average droplet volumetric heating is the absorbed power divided by the droplet volume, but the volumetric heating is a function of radial position within the droplet.

RADIAL DEPENDENCE OF ABSORPTION

The intensity attenuation, equation (17a), can be expressed as a function of the radial position, r (see Fig. 2), by replacing s with

$$s = R\{\cos\phi \pm [(r/R)^2 - \sin^2\phi]^{1/2}\} \tag{29}$$

from the law of cosines, where R is the droplet radius. Note that values of r less than $R\sin\phi$ are not on the ray path, and each value of r on the ray path occurs twice on one traversal of the droplet. The intensity of a single ray on the first traversal is then

$$I_{\pm}(r) = I_0 \exp(-KR\{\cos\phi \pm [(r/R)^2 - \sin^2\phi]^{1/2}\}) \quad \text{for} \quad r \geqslant R\sin\phi \tag{30}$$

$$I_{\pm}(r) \equiv 0 \quad \text{for} \quad r < R\sin\phi.$$

The absorption distribution for each of the infinite series of droplet traversals by a single ray will have the same radial dependence as the first traversal. Thus, the fraction of the absorption of a single ray occurring in the spherical shell $r_1 \leqslant r \leqslant r_2$ is

$$\alpha(r_1, r_2) = \frac{I_-(r_2) - I_-(r_1) + I_+(r_1) - I_+(r_2)}{I_-(R) - I_+(R)}. \tag{31}$$

The total power absorbed in this shell is obtained by multiplying α in equation (25) by $\alpha(r_1, r_2)$ of equation (31), thus integrating over rays of all incident angles and wavelengths. The volumetric heating in this shell is then the power absorbed minus the power emitted by the shell divided by the shell volume, $\frac{4}{3}\pi(r_2^3 - r_1^3)$. For an isothermal droplet, the local emitted power is what the local absorbed power would be for T_B at the droplet temperature.

DROPLET EVAPORATION RATE

Simple correlations for droplet drag and convective heating can be used with the present determinations of radiative heating to demonstrate evaporation rates and the relative magnitudes of radiative and convective heating.

In many typical nuclear reactor accident scenarios water droplets are heated in very hot water vapor with a fairly low concentration of noncondensable gas. A droplet so situated reaches or becomes near the saturation temperature relatively quickly. Further heating causes evaporation; as shown in the following section, there would be negligible internal superheating. The evaporative mass flux at the surface is

$$\dot{m}'' = \frac{q}{h_{fg}} \tag{32}$$

where h_{fg} is the heat of vaporization and $q = q_r + q_c$ is the combined radiative and convective heat flux. The time rate of change of the droplet size is

$$\frac{1}{2}\frac{\mathrm{d}D}{\mathrm{d}t} = -\frac{q}{\rho_l h_{fg}} \tag{33}$$

where ρ_l is the liquid density. This rate of change is integrated to obtain the evaporation time

$$t_{\text{evap}} = \frac{\rho_l h_{fg}}{2} \int_{D(t)}^{D_0} \frac{\mathrm{d}D}{(q_r + q_c)}. \tag{34}$$

The radiative heat flux for black body surrounds at temperature T_B is

$$q_r = \alpha_{\text{eff}}(T_B)\sigma T_B^4 - \alpha_{\text{eff}}(T_{\text{sat}})\sigma T_{\text{sat}}^4, \tag{35}$$

because the droplet emissivity is $\alpha_{\text{eff}}(T_{\text{sat}})$ from Kirchhoff's law.

The Reynolds number and Nusselt number of an evaporating droplet are generally functions of time. However, this unsteady convection can usually be well approximated using a quasi-steady approach, as has been shown for droplets falling from rest [23–25] and in situations with much larger accelerations [26]. The time constants in fall from rest are shorter than the evaporation rate time constants even when the ambient temperature is 1450 K.

The steady state drag coefficient for rigid spheres, defined as

$$c_d = \frac{d}{1/2\rho_v U^2 A_c} \tag{36}$$

where d is the drag, ρ_v the ambient density, U the relative free stream velocity, and $A_c = \pi R^2$, is well correlated [27] by the simple relation

$$c_d = 0.2924(1 + 9.06/Re_D^{1/2})^2. \tag{37}$$

Yuen and Chen [28] show that this rigid sphere drag also holds approximately for evaporating droplets; the effect of blowing (normal velocity at the surface) on c_d can be neglected for the present purposes. Their explanation is that although viscous drag is reduced by blowing, pressure drag is increased, because separation occurs earlier with blowing.

The droplet acceleration is found to be

$$\ddot{x} = g\left(1 - \frac{\rho_v}{\rho_l}\right) - \frac{3}{4}\frac{\mu^2}{\rho_v \rho_l D^3} Re_D^2 c_d \tag{38}$$

from a simple force balance. The Reynolds number as a function of time is obtained by integrating equation (38)

$$Re_D(t) = \frac{\rho_v U D}{\mu} = Re_D(0) + \frac{\rho_l g D}{\mu}\left(1 - \frac{\rho_v}{\rho_l}\right)t - \frac{3}{4}\frac{\mu D}{\rho_l}\int_0^t \frac{Re_D^2 c_d}{D^3}\,\mathrm{d}t. \tag{39}$$

This droplet Reynolds number can be approximated by the terminal Reynolds number if $\ddot{x}$ is much less than g. From equations (37) and (38) the terminal Reynolds number is

$$Re_D = \left\{-4.53 + \left[20.52 + 2.135\frac{[D^3 g \rho_v(\rho_l - \rho_v)]^{1/2}}{\mu}\right]^{1/2}\right\}^2. \tag{40}$$

Table 1. Effective absorptance, α_{eff}

D [mm]/T_B [K] =	373	450	650	850	1050	1250	1450
∞	0.919	0.925	0.930	0.932	0.932	0.933	0.934
3.0	0.919	0.924	0.930	0.930	0.924	0.908	0.881
2.0	0.919	0.924	0.930	0.927	0.915	0.892	0.858
1.0	0.919	0.924	0.928	0.918	0.893	0.854	0.805
0.5	0.919	0.924	0.924	0.905	0.865	0.809	0.745
0.2	0.917	0.920	0.910	0.871	0.810	0.735	0.656
0.1	0.907	0.902	0.870	0.815	0.740	0.657	0.575
0.05	0.865	0.844	0.782	0.714	0.637	0.557	0.481
0.02	0.726	0.680	0.592	0.530	0.470	0.410	0.352
0.0	0.000	0.000	0.000	0.000	0.000	0.000	0.000

The average Nusselt number for a sphere without blowing is well correlated by [29]

$$Nu_D^+ = \frac{q_c^+ D}{k(T_v - T_{sat})} = 1.56 + 0.616 Re_D^{1/2} Pr^{1/3} \quad \text{for} \quad Re_D Pr^{2/3} \geq 2 \quad (41a)$$

$$= 2.00 + 0.216 Re_D Pr^{2/3} \quad \text{for} \quad Re_D Pr^{2/3} < 2. \quad (41b)$$

A very common heat-transfer blowing correction invoked for evaporating droplets [30] is

$$q_c = q_c^+ \frac{\ln(1+B)}{B} \quad (42)$$

where the superheat parameter is

$$B = \frac{c_{pv}(T_v - T_{sat})}{h_{fg} - q_r/\dot{m}''} = \frac{c_{pv}(T_v - T_{sat})}{h_{fg}} \left(1 + \frac{q_r}{q_c}\right) \quad (43)$$

and where c_{pv} is the heat capacity at constant pressure evaluated at the ambient temperature. The thermal conductivity, k, and the viscosity, μ, have often been successfully evaluated at the "1/3 rule" reference temperature [28], $T_{ref} = T_{sat} + (T_v - T_{sat})/3$.

RESULTS AND CONCLUSIONS

The present ray tracing procedure and that of Edwards [22] for thick plane parallel layers are algebraically very different, but in actual physical modeling, they differ only in how the phase of the electromagnetic radiation is handled. In the present procedure, the phase is ignored or effectively averaged before the ray encounters any surface. Edwards retains the phase in his ray tracing, which allows interference effects, then he averages over phase by integrating after the ray tracing is completed. A computer code was obtained from Edwards which computes perpendicular and parallel components of transmittance, reflectance, and absorptance for a thick parallel layer using his approach; another computer code was written which computes the same parameters using the present analysis. Due to analogous symmetries, the parallel layer absorption problem is nearly identical to the sphere absorption problem. Runs were made with the two codes for layer thicknesses of 0.1 and 0.5 mm, with the optical properties of water, at various incident angles and wavelengths. In all cases, the results of the two codes were identical to five or six significant figures.

The effective absorptance of water droplets has been computed for black body temperatures from 373 to 1450 K and droplet diameters from 0.02 to 3.0 mm (see Table 1). The integrals in equation (25) were evaluated using the trapezoidal rule with 50 equal divisions of θ and with 157 different wave lengths from 0.5 to 200 μm (at those values in [15] where the complex refractive index is tabulated). It can be seen from Table 1 that water droplets absorb very strongly. The effective absorptance is only weakly dependent on the black body temperature, but the effective absorptance is generally greater for

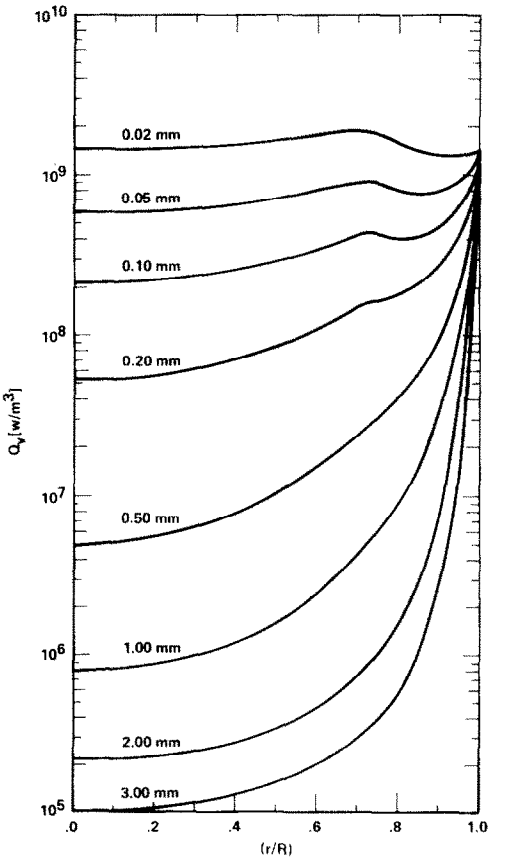

FIG. 3. Radial dependence of volumetric heating, $T_B = 650$ K.

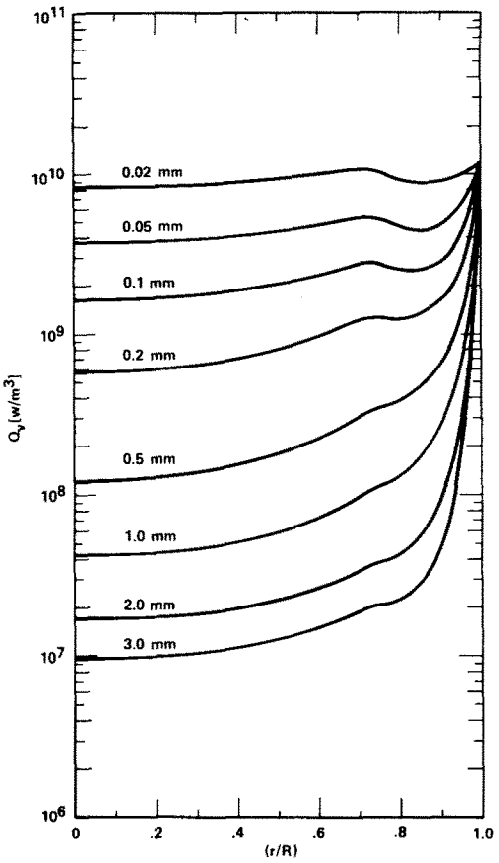

FIG. 4. Radial dependence of volumetric heating, $T_B = 1050$ K.

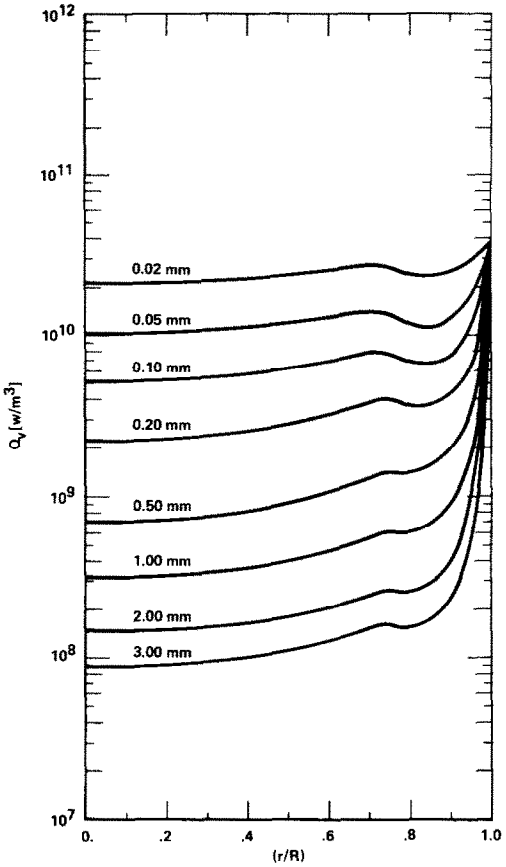

FIG. 5. Radial dependence of volumetric heating, $T_B = 1450$ K.

lower black body temperatures. The emissivity of an isothermal droplet, from Kirchhoff's law, is the effective absorptance evaluated at the droplet temperature.

The volumetric heating as a function of radial position has been computed using equation (31) with twenty equal radial divisions of the droplet (see Figs. 3–5), for black body temperatures 650, 1050 and 1450 K, for an isothermal droplet temperature of 373 K, and for a range of droplet diameters. The same 157 wave number divisions and 50 equal angular divisions as mentioned previously were used for these computations. Most rays in the black body distribution are strongly attenuated and do not

Table 2. Cumulative evaporation time (s) for water droplets at their instantaneous terminal velocity with $T_v = T_B$

D [mm]/T_B [K] =	450	650	850	1050	1250	1450
3.0	0.0	0.0	0.0	0.0	0.0	0.0
2.8	12.2	3.47	1.94	1.27	0.885	0.640
2.6	24.3	6.90	3.85	2.52	1.76	1.28
2.4	36.1	10.3	5.75	3.76	2.63	1.91
2.2	47.8	13.6	7.61	4.98	3.50	2.54
2.0	59.2	16.7	9.45	6.19	4.35	3.16
1.8	70.4	20.1	11.3	7.38	5.19	3.78
1.6	81.4	32.2	13.0	8.55	6.03	4.40
1.4	92.1	26.3	14.8	9.70	6.85	5.00
1.2	102.0	29.3	16.4	10.8	7.65	5.60
1.0	112.0	32.1	18.1	11.9	8.44	6.19
0.8	122.0	34.9	19.7	13.0	9.21	6.77
0.6	131.0	37.6	21.2	14.0	9.94	7.32
0.4	140.0	40.0	22.6	14.9	10.6	7.84
0.2	147.0	42.2	23.8	15.7	11.2	8.30
0.1	150.0	42.9	24.2	16.0	11.4	8.45
0.01	151.0	43.3	24.4	16.1	11.5	8.51
0.00	151.0	43.3	24.4	16.1	11.5	8.51

Table 3. Fall distance (m) of evaporating water droplets during their lifetime with $T_v = T_B$

D [mm]/T_B [K] =	450	650	850	1050	1250	1450
3.0	1246.0	401.8	243.8	169.2	124.1	92.98
2.8	1089.0	350.6	212.3	147.2	107.9	80.88
2.6	941.6	302.2	182.7	126.5	92.70	69.48
2.4	803.8	257.2	155.2	107.3	78.55	58.86
2.2	675.4	215.4	129.6	89.44	65.42	49.01
2.0	557.6	177.1	106.2	73.13	53.42	40.00
1.8	450.1	142.2	84.96	58.33	42.54	31.82
1.6	353.4	111.0	65.97	45.13	32.83	24.52
1.4	267.3	83.31	49.22	33.51	24.31	18.13
1.2	192.6	59.42	34.83	23.57	17.03	12.67
1.0	129.6	39.45	22.87	15.35	11.02	8.17
0.8	78.5	23.46	13.39	8.88	6.32	4.66
0.6	40.1	11.62	6.48	4.22	2.97	2.17
0.4	14.5	4.01	2.15	1.36	0.93	0.67
0.2	2.1	0.51	0.25	0.15	0.10	0.07
0.1	0.2	0.04	0.02	0.01	0.00	0.00
0.01	0.0	0.00	0.00	0.00	0.00	0.00

Table 4. Heat flux ratio, q_r/q_c, for water droplets at their instantaneous terminal velocity with $T_v = T_B$

D [mm]/T_B [K] =	450	650	850	1050	1250	1450
3.0	0.069	0.157	0.314	0.584	1.05	1.88
2.8	0.068	0.155	0.310	0.574	1.03	1.83
2.6	0.067	0.152	0.304	0.563	1.00	1.78
2.4	0.066	0.150	0.300	0.551	0.982	1.72
2.2	0.065	0.147	0.293	0.539	0.954	1.66
2.0	0.063	0.144	0.286	0.525	0.924	1.60
1.8	0.062	0.141	0.279	0.510	0.892	1.53
1.6	0.061	0.137	0.271	0.493	0.857	1.45
1.4	0.059	0.133	0.264	0.477	0.825	1.38
1.2	0.057	0.129	0.254	0.457	0.781	1.29
1.0	0.055	0.124	0.243	0.433	0.729	1.18
0.8	0.052	0.118	0.229	0.404	0.669	1.06
0.6	0.049	0.110	0.213	0.369	0.599	0.920
0.4	0.045	0.098	0.185	0.311	0.484	0.707
0.2	0.036	0.075	0.134	0.210	0.298	0.393
0.1	0.025	0.046	0.074	0.105	0.139	0.172
0.03	0.007	0.012	0.019	0.026	0.033	0.039
0.01	0.001	0.002	0.003	0.004	0.005	0.006

penetrate far past the surface. Rays at some wave numbers are only weakly absorbed. These weakly absorbed rays are focused toward the center, which explains the relative maximum in volumetric heating in the $0.7 < (r/R) < 0.8$ region which occurs for the smaller droplets.

To demonstrate typical relative magnitudes of radiative heat flux and convective heat flux, and to demonstrate typical evaporation times, these parameters were computed for water droplets falling at their instantaneous terminal velocity relative to pure superheated water vapor at a pressure of one bar. The ambient vapor temperature was taken to be equal to the black body radiating temperature. The fluid properties were taken from [31] with μ, k, and Pr evaluated at the "1/3 rule" reference temperature and ρ_v evaluated at the ambient temperature. For a given temperature of the surrounds, the droplet evaporation rate, dD/dt, is approximately constant for droplets larger than 1 mm, while dD^2/dt is nearly constant for droplets smaller than 0.1 mm. The total evaporation of an initially 1–3 mm diameter droplet takes tens of seconds, while the total evaporation of a 0.1 mm droplet takes tenths of seconds (see Table 2). The fall distance of evaporating droplets during their lifetime is given in Table 3. The radiative heat flux is generally very significant compared with the convective heat flux, for temperatures above 450 K, unless the droplet diameter is less than 30 μm (see Table 4). The radiative heat transfer to the droplet can actually be greater than the convective heat transfer if the temperature of the surrounds is above about 1250 K.

The assumption that the droplet falls at its instantaneous terminal velocity is the same as the assumption that the fall velocity does not depend on past history; this holds when the acceleration, $\ddot{x}$, is much less than g. In the just described evaporation

computations, the highest acceleration (at 1450 K) was $\ddot{x} = -0.3\,g$. If history effects were included for this 1450 K case, starting with a 3 mm droplet at its terminal velocity, the instantaneous Reynolds numbers would be only as much as 7% higher for this extreme case. The maximum acceleration for other surround temperatures can be estimated by proportioning the evaporation times. The instantaneous terminal velocity approximation is usually very good.

Acknowledgement—This work was supported by a grant from the National Science Foundation.

REFERENCES

1. M. S. Bhatti, Dynamics of a vaporizing droplet in laminar entry region of a straight channel, *J. Heat Transfer* **99**, 574–579 (1977).
2. H. A. Frediani, Jr and N. Smith, Mathematical model for spray cooling systems, *J. Engng Pwr* **99**, 279–283 (1977).
3. I. S. Habib, The interaction of a hot gas flow and a cold liquid spray, *J. Heat Transfer* **98**, 421–426 (1976).
4. W. H. Gauvin, S. Katta and F. H. Knelman, Drop trajectory predictions and their importance in the design of spray dryers, *Int. J. Multiphase Flow* **1**, 793–816 (1975).
5. P. H. Rothe and J. A. Block, Aerodynamic behavior of liquid sprays, *Int. J. Multiphase Flow* **3**, 263–272 (1977).
6. C. Peterson, Literaturübersicht über einige Eigenschaften von Zircaloy-4 bei hoheren Temperaturen, KFK-Ext. 6/73-6 (1974).
7. G. Mie, Optics of turbid media, *Ann. Phys.* **25**, 377–445 (1908).
8. H. C. van der Hulst, *Light Scattering by Small Particles*. John Wiley, New York (1957).
9. G. N. Plass, Mie scattering and absorption cross sections for absorbing particles, *Appl. Optics* **5**, 279–285 (1966).
10. P. Chýlek, Large sphere limits of the Mie-scattering functions, *J. Opt. Soc. Am.* **63**, 699–706 (1973).
11. D. Deirmendjian, *Electromagnetic Scattering on Spherical Polydispersions*. Elsevier, New York (1969); also RAND report R-456-PR.
12. S. H. Chan and M. A. Grolmes, Hydrodynamically-controlled rewetting, *Nucl. Engng Design* **34**, 307–316 (1975).
13. K. N. Liou and J. E. Hansen, Intensity and polarization for single scattering by polydisperse spheres: a comparison of ray optics and Mie theory, *J. Atmos. Sci.* **28**, 995–1004 (1971).
14. H. C. Simpson, Combustion of droplets of heavy liquid fuels, Sc.D. Thesis in Chem. Engng, MIT, Cambridge, Mass. (1954); also reported in *Symposium (International) on Combustion (Fifth)*, pp. 101–129 (1954); also reported in H. C. Hottel and A. F. Sarofim, *Radiative Transfer*, pp. 390–391. McGraw-Hill, New York (1967).
15. G. M. Hale and M. R. Querry, Optical constants of water in the 200-nm to 200-μm wavelength region, *Appl. Optics* **12**, 555–563 (1973).
16. P. S. Ray, Broadband complex refractive indices of ice and water, *Appl. Optics* **11**, 1836–1844 (1972).
17. G. M. Hale, M. R. Querry, A. N. Rusk and D. Williams, Influence of temperature on the spectrum of water, *J. Opt. Soc. Am.* **62**, 1103–1108 (1972).
18. L. W. Pinkley, P. P. Sethna and D. Williams, Optical constants of water in the infrared: influence of temperature, *J. Opt. Soc. Am.* **67**, 494–499 (1977).
19. R. J. Bell, K. R. Armstrong, C. S. Nichols and R. W. Bradley, Generalized laws of refraction and reflection, *J. Opt. Soc. Am.* **59**, 187–189 (1969).
20. J. A. Stratton, *Electromagnetic Theory*. McGraw-Hill, New York (1941).
21. R. Siegel and J. R. Howell, *Thermal Radiation Heat Transfer*, pp. 90–92 and 415. McGraw-Hill, New York (1972).
22. D. K. Edwards, Radiative transfer characteristics of materials, *J. Heat Transfer* **91**, 1–15 (1969).
23. K. V. Beard, On the acceleration of large water drops to terminal velocity, *J. Appl. Meteor.* **16**, 1068–1071 (1977).
24. P. K. Wang and H. R. Pruppacher, Acceleration to terminal velocity of cloud and raindrops, *J. Appl. Meteor.* **16**, 275–280 (1977).
25. J. D. Sartor and C. E. Abbott, Prediction and measurement of the accelerated motion of water drops in air, *J. Appl. Meteor.* **14**, 232–239 (1975).
26. W. P. Manning and W. H. Gauvin, Heat and mass transfer to decelerating finely atomized sprays, *A.I.Ch.E. Jl* **6**, 184–190 (1960).
27. F. F. Abraham, Functional dependence of drag coefficient of a sphere on Reynolds number, *Physics Fluids* **13**, 2194–2195 (1970).
28. M. C. Yuen and L. W. Chen, On drag of evaporating liquid droplets, *Combust. Sci. Technol.* **14**, 147–154 (1976).
29. K. V. Beard and H. R. Pruppacher, A wind tunnel investigation of the rate of evaporation of small water drops falling at terminal velocity in air, *J. Atmos. Sci.* **28**, 1455–1464 (1971).
30. D. B. Spalding, Combustion in liquid-fuel rocket motors, *Aeronaut. Q.* **10**, 1–27 (1959).
31. E. Schmidt, *Properties of Water and Steam in SI Units*. Springer, New York (1969).

ABSORPTION RADIATIVE PAR EVAPORATION DE GOUTTELETTES

Résumé—Le chauffage volumique du à l'absorption radiative est calculé en fonction de la position radiale de gouttelettes sphériques d'eau dans un environnement de corps noir, à des températures allant jusqu'à 1450 K. L'absorptance effective de la goutte et le temps d'évaporation à partir d'un diamètre de référence a été calculé et tabulé. En prenant des différences entre entrées de la table, le temps pour évaporer d'un diamètre à un autre peut être trouvé. La procédure développée pour ces calculs inclut la polarisation, la réfraction, la réflexion externe, les réflexions multiples internes et l'absorption.

STRAHLUNGSABSORPTION DURCH VERDAMPFUNG VON TRÖPFCHEN

Zusammenfassung—Die Erwärmung eines Volumens durch Strahlungsabsorption wurde als Funktion der radialen Position für kugelförmige Wassertropfen in der Umgebung von schwarzen Körpern mit Temperaturen bis zu 1450 K berechnet. Die effektive Absorption des Tröpfchens und die Verdampfungszeit von einem Referenzdurchmesser bis zu beliebigen kleineren Durchmessern wurde berechnet und tabelliert. Durch Interpolation zwischen den Eingangswerten der Tabelle kann die Zeit für die Verdampfung von einer Größe zur nächsten gefunden werden. Bei der Berechnung der Strahlungsvorgänge wurden Polarisation, Brechung, äußere Reflexion, mehrfache innere Reflexion und Absorption berücksichtigt.

ПОГЛОЩЕНИЕ ИЗЛУЧЕНИЯ ИСПАРЯЮЩИМИСЯ КАПЛЯМИ

Аннотация — Рассчитан объёмный нагрев сферических капель воды, обусловленный поглощением излучения от черного тела при температурах вплоть до 1450 К как функция радиальной координаты. Рассчитаны также и затобулированы эффективная поглощательная способность капли и время, за которое диаметр капли меняется от начального до заданного значения. Данные, представленные в таблице, позволяют рассчитать время испарения от одного размера до другого. Лучевой подход, развитый для этих расчётов, включает поляризацию, рефракцию, внутреннее отражение, многократные внутренние отражения и поглощение.